INTERNATIONAL JOURNAL FOR NUMERICAL METHODS IN FLUIDS
Int. J. Numer. Meth. Fluids 2009; **60**:295–322
Published online 13 August 2008 in Wiley InterScience (www.interscience.wiley.com). DOI: 10.1002/fld.1888

A convective weakly viscoelastic rotating flow with pressure Neumann condition

Julio R. Claeyssen[1,*,†], Elba Bravo Asenjo[2] and Obidio Rubio[3]

[1]*IM-Promec, Universidade Federal do Rio Grande do Sul, P.O. Box 10673, 90001-970 Porto Alegre, RS, Brazil*
[2]*UNASP-Adventist University Center of São Paulo, SP, Brazil*
[3]*Facultad de Ciencias, Universidad Nacional de Trujillo, La Libertad, Peru*

SUMMARY

The objective of this work is to investigate through the numeric simulation, the effects of the weakly viscoelastic flow within a rotating rectangular duct subject to a buoyancy force due to the heating of one of the walls of the duct. A direct velocity–pressure algorithm in primitive variables with a Neumann condition for the pressure is employed. The spatial discretization is made with finite central differences on a staggered grid. The pressure field is directly updated without any iteration. Numerical simulations were done for several Weissemberg numbers (We) and Grashof numbers (Gr). The numerical results show that for high Weissemberg numbers ($We > 7.4 \times 10^{-5}$) and for ducts with aspect ratio 2:1 and 8:1, the secondary flow is restabilized with a stretched double vortex configuration. It is also observed that when the Grashof number is increased ($Gr > 17 \times 10^{-4}$), the buoyancy force neutralizes the effects of the Coriolis force for ducts with aspect ratio 8:1. Copyright © 2008 John Wiley & Sons, Ltd.

Received 13 August 2007; Revised 22 June 2008; Accepted 23 June 2008

KEY WORDS: non-Newtonian; incompressible flow; mixed convection; rotating flow; finite differences methods; pressure Neumann condition

1. INTRODUCTION

This work seeks to study the internal weakly viscoelastic flow contained in a rotating rectangular duct with buoyancy effects due to the heating of a wall of the duct. This is done with a direct pressure–velocity algorithm in primitive variables [1] that considers a pressure Neumann condition. This later condition is important for updating the pressure in one step without any iteration. Central differences on a staggered grid are employed because they allow second-order approximations.

*Correspondence to: Julio R. Claeyssen, IM-Promec, Universidade Federal do Rio Grande do Sul, P.O. Box 10673, 90001-970 Porto Alegre, RS, Brazil.
†E-mail: julio@mat.ufrgs.br

Copyright © 2008 John Wiley & Sons, Ltd.

The Navier–Stokes equations, together with the divergence free condition, constitute the basic formulation for an incompressible flow. From a mathematical point of view, the system that governs this kind of flow is singular with respect to the pressure. There is no evolution equation for such a quantity. Following the work of Gresho and Sani [2], the pressure is obtained by solving a Poisson equation with a Neumann boundary condition. A compatibility condition of the source with the boundary conditions guarantees the existence of solutions.

The internal rotating flow problem has been considered by several authors: Chen *et al*. [3], Speziale [4, 5], Robertson [6], Khayat [7], Jin and Chen [8], Nonino and Comini [9], Nonino and Croce [10], Liqiu [11], Lee and Yan [12], among others. Speziale employed the divergence-vorticity formulation with finite-difference schemes due to Arakawa for the convective terms and the DuFort–Frankel scheme for the viscous-diffusion terms. Chen *et al*. employed Fourier–Chebyshev pseudo-spectral methods for solving incompressible flows in 3D channels in rotation with square traversal section. Robertson performed numerical studies for laminar incompressible flows in curved ducts. He employed finite differences on a staggered grid with Newton method. Khayat studied thermal convection with viscoelastic fluids that satisfy the constitutive equations of Oldroy-B. By using the stream function–vorticity formulation, Jin and Chen [8] considered a numerical study for the transient behavior of the natural convection in a vertical rectangular region. Nonino and Comini [9] and Nonino and Croce [10] treated the problem of the natural convection by using the finite element method. Liqiu [11] considered a stationary study of the transition of the buoyancy forces due to the rotation of a curved duct with a square transverse section, rotating around a perpendicular axis to the extension of the duct. Lee and Yan [12] investigated mixed convection heat and mass transfer in the entrance region of radial rotating rectangular ducts with water film evaporation along the porous duct walls by using a vorticity–velocity numerical method. Emphasis was placed on the rotation effects, including both Coriolis and centrifugal buoyancy forces and the mass diffusion effect on the flow structure and heat transfer characteristics.

The understanding of the pressure-driven flow of a viscoelastic fluid flow is of importance in many industrial processes such as fiber spinning, injection molding, extrusion and in the design of various types of rotating machinery. The addition of a minute amount of a long chain polymer (e.g. 50–100 parts/million by weight) to a Newtonian liquid produces a highly dilute viscoelastic liquid which can be considerably more stable in the presence of rotations [5]. In turbulent pipe flows it results in a substantial decrease in the pressure drop. The prediction of this behavior requires adoption of appropriate constitutive equations and rheological parameters. Since the parameters in the constitutive equation determine the viscoelastic characteristics of flow, i.e. secondary flow patterns and volumetric flow rates, numerical prediction or measurements of velocity at certain locations can be used to estimate these parameters [13, 14].

This work will be focused on the structure of the secondary flow and its effects on the flow in the axial direction of the duct. It is assumed that the duct is long enough to suppress effects at the end so that the secondary flow is independent of the coordinate along the axial direction. We shall consider two problems. The first one refers to the case of a weakly viscoelastic rotating flow that is studied for several Weissemberg numbers [4, 5] in ducts with aspect ratio 2:1 and 8:1. The other one is a mixed convection problem with a weakly viscoelastic rotating flow for several Grashof numbers in ducts of aspect ratio 8:1.

With the Neumann pressure condition, the results obtained by Speziale [5] for a rotating flow have been reproduced. Specific calculations shows that the addition of small amounts of a long chain polymer to Newtonian liquid can have a stabilizing effect on rotating channel flow and give rise to secondary flows with a substantially reduced frictional drag. This is a non-linear effect

Copyright © 2008 John Wiley & Sons, Ltd.

DOI: 10.1002/fld

which, although observed experimentally in analogous flow configurations, to our knowledge has not been calculated in rotating channel flow. The computational experiences with temperature effects allows observation of how the heat supplied by some mechanism generates flow instability with respect to earlier configurations.

2. THE GOVERNING EQUATIONS

In this section, we present in compact form the equations for an incompressible fluid subject to a forcing term that will characterize the problems to be discussed in this work.

With the objective to write the equations in non-dimensional form we introduce the following scales: D the length scale, W_0 the velocity scale, $\Delta T = T_h - T_0$ the temperature difference and the P_0 pressure scale. We then consider the following non-dimensional variables:

$$x_1 \to D_x, \quad x_2 \to D_y, \quad x_3 \to D_z, \quad t^* \to \frac{D}{W_0}t, \quad v_1 \to W_0 u$$

$$v_2 \to W_0 v, \quad v_3 \to W_0 w, \quad T \to \frac{T - T_0}{\Delta t}, \quad p^* \to P_0 P$$

The non-dimensional numbers $Re = W_0 D/\nu, Pe = W_0 D/\alpha$ are the Reynolds number and the Peclet number, respectively. Here ν denotes the kinematic viscosity and α is the thermal diffusion coefficient. Then the non-dimensional equations that govern the flow of an incompressible fluid are given by the momentum equation

$$\frac{\partial \mathbf{u}}{\partial t} + \mathbf{u}\cdot\nabla\mathbf{u} + \nabla P = \frac{1}{Re}\nabla^2\mathbf{u} + \mathbf{F}(\mathbf{u},\theta) \quad \text{in } \Omega, \ t>0 \tag{1}$$

the continuity equation

$$\nabla\cdot\mathbf{u} = 0 \quad \text{in } \Omega, \ t>0 \tag{2}$$

and the energy equation

$$\frac{\partial \theta}{\partial t} + \mathbf{u}\cdot\nabla\theta = \frac{1}{Pe}\nabla^2\theta \quad \text{in } \Omega, \ t>0 \tag{3}$$

In these equations, Ω is a spatial region limited by the contour Γ, $\mathbf{u} = \mathbf{u}(t,\mathbf{x}) = (u(t,\mathbf{x}), v(t,\mathbf{x}), w(t,\mathbf{x}))$, $P = P(t,\mathbf{x})$ and $\theta = \theta(t,\mathbf{x})$ are, respectively, the velocity, the pressure, the temperature of the fluid and $\mathbf{F}$ is a forcing term given below for the two Maxwell viscoelastic models that are considered in this work and to be discussed in more detail in Sections 6 and 7.

- *Model I*: Rotating weakly viscoelastic flow

$$\mathbf{F}(\mathbf{u}) = (2/Ro)\mathbf{j}\times\mathbf{u} - 2We(\nabla^2 w\nabla w + \tfrac{1}{2}\nabla(\nabla w)^2) \tag{4}$$

  where $Ro = W_0/\omega D$ is the Rossby number and $We = \lambda\nu/D^2$ is the Weissemberg number, satisfying $We \ll 1$.
- *Model II*: Rotating mixed convective weakly viscoelastic flow

$$\mathbf{F}(\mathbf{u},\theta) = (2/Ro)\mathbf{j}\times\mathbf{u} - 2We(\nabla^2 w\nabla w + \tfrac{1}{2}\nabla(\nabla w)^2) + \frac{Gr}{Re^2}\theta\mathbf{j} \tag{5}$$

Copyright © 2008 John Wiley & Sons, Ltd.

DOI: 10.1002/fld

where $Gr = g\beta\Delta T D^3/\nu^2$ is the Grashof number, g is the gravity acceleration and β is the coefficient of thermal expansion.

Here, the rotating vector, $\boldsymbol{\omega} = \omega j$ is in the direction of the y-axis, where ω is the angular velocity.

The problem under consideration deals with a weakly viscoelastic incompressible fluid flow contained in a rectangular duct, driven by the pressure and subject to a permanent rotation in the direction perpendicular to the duct as considered in [4, 15]. The physical configuration and coordinate system are shown in Figure 1.

Equations (1)–(2) are subject to the following initial and boundary conditions

$$\mathbf{u}(0, \mathbf{x}) = \mathbf{u}_0(\mathbf{x}), \quad \mathbf{x} \text{ in } \overline{\Omega} = \Omega \cup \Gamma \tag{6}$$

$$\mathbf{u} = \mathbf{u}_\Gamma(\mathbf{x}, t) \quad \text{on } \Gamma = \partial\Omega \tag{7}$$

where $\mathbf{u}_0$ satisfies the continuity equation

$$\nabla . \mathbf{u}_0 = 0 \quad \text{in } \Omega \tag{8}$$

and $\mathbf{u}_0$, $\mathbf{u}_\Gamma$ being subject to the restriction

$$\mathbf{u}_0 \cdot n = \mathbf{u}_\Gamma(0, \mathbf{x}) \cdot n \quad \text{on } \Gamma \tag{9}$$

From the continuity equation and the divergence theorem, it follows the condition of global mass

$$\int_\Gamma \mathbf{u} \cdot n \, \mathrm{d}x = 0 \tag{10}$$

where n is the unit exterior normal to the boundary Γ of the region Ω.

In agreement with Ladyzhenskaya [16], the specification of the pressure at the non-slip wall of Γ is not allowed. Otherwise, the system (1)–(10) would be over determined. It is clear from Equations (1)–(2), that there is no explicit equation for the pressure. The velocity field, in principle, calculated from the momentum equation must be restricted so that it satisfies the solenoidal kinematic

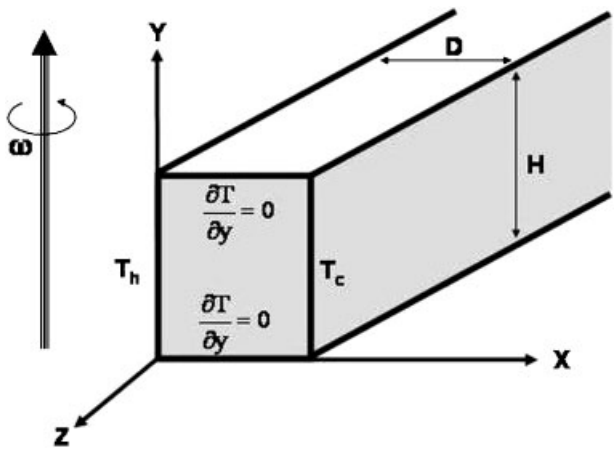

Figure 1. Flow in a rotating rectangular duct.

Copyright © 2008 John Wiley & Sons, Ltd.

DOI: 10.1002/fld

condition $\nabla\cdot\mathbf{u}=0$. This means that the pressure has two contributions; influences it serves as a force for conservation in the mechanical balance law but, also, as a continuity restriction [17].

For the energy Equation (3), the initial conditions are given

$$\theta(\mathbf{x},0)=\theta_0(\mathbf{x}),\quad \mathbf{x}\text{ in }\Omega \tag{11}$$

and the mixed boundary conditions

$$\theta=\theta_{\Gamma_1}(\mathbf{x},t)\quad \text{on }\Gamma_1\subset\Gamma \tag{12}$$

$$\frac{\partial\theta}{\partial n}=\theta_{\Gamma_2}(\mathbf{x},t)\quad \text{on }\Gamma_2\subset\Gamma \tag{13}$$

where $\Gamma=\Gamma_1\cup\Gamma_2$ is the boundary of the region Ω. Here Γ_1 refers to the vertical walls of the duct and Γ_2 refers to the horizontal ones.

2.1. The Poisson equation for the pressure

By applying the divergence operator in Equation (2), together with the momentum Equation (1), leads to the pressure equation

$$\nabla^2 P=\nabla\cdot\left(\frac{1}{Re}\nabla^2\mathbf{u}-\mathbf{u}\cdot\nabla\mathbf{u}+\mathbf{F}(\mathbf{u},\theta)\right)\quad \text{in }\Omega\ \text{ for } t\geqslant 0 \tag{14}$$

Thus, the pressure is determined by solving a Poisson equation subject to appropriate boundary conditions. For the problem to be well-posed, the boundary conditions must be given in such a way that the continuity equation is satisfied near the boundary. To keep the divergence-free condition for the velocity is an important requirement for the simulation of an incompressible flow.

The above equation is actually employed as a substitute for the continuity equation. The elliptic nature of this equation forces the need of prescribing a boundary condition for the pressure. In a fundamental work by Gresho and Sani [2], it is concluded that a Neumann condition for the pressure turns out to be the most appropriate. This condition is obtained by taking the normal component of the pressure gradient isolated from the momentum equation, that is

$$\frac{\partial P}{\partial n}=n\cdot\nabla P=n\cdot\left(\frac{1}{Re}\nabla^2\mathbf{u}-\frac{\partial\mathbf{u}}{\partial t}-\mathbf{u}\cdot\nabla\mathbf{u}+\mathbf{F}(\mathbf{u},\theta)\right)\quad \text{on }\Gamma\ \text{ for } t\geqslant 0 \tag{15}$$

In order that a Poisson equation (14) with a Neumann condition (15) can be solved, it is necessary that the following compatibility condition be satisfied

$$\int\!\!\int_{\Omega}\nabla^2 P\,\mathrm{d}\Omega=\int_{\Gamma}P_n\,\mathrm{d}\Gamma \tag{16}$$

where $P_n=n\cdot\nabla P$.

Copyright © 2008 John Wiley & Sons, Ltd.

DOI: 10.1002/fld

3. DISCRETIZATION OF THE NAVIER–STOKES EQUATIONS

When the duct is assumed to be sufficiently long, there is an internal section where the effects at the extremes can be neglected, that is, the flow is fully developed. The axial pressure gradient

$$\frac{\partial P}{\partial z} = -G$$

is considered constant, maintained by external means (P is the modified pressure, which includes the gravitational and centrifugal force potentials). In this situation, it is observed that in the internal region, the physical properties of the flow become independent of the coordinate z; however, the fully developed velocity field is three-dimensional. For non-zero rotation rates, the components $u,\ v$ of the velocity $\mathbf{v}=(u,v,w)$ are termed the secondary flow and the component w is referred to as the main flow.

With the above considerations, Equations (1) and (3) will be discretized with central finite differences on a staggered grid $x_i = i\Delta x, y_j = j\Delta y; i=1,\ldots,N, j=1,\ldots,M$ on the transverse section of the duct [18]. The spatial approximations for the pressure P, temperature θ and the main velocity w are taken at the center of each cell. The first-order derivatives can be approximated by forward or central differences. The notation $D_{1r}, D_{2r}, r=x, y$, is employed for the first-order forward difference operator and for the second-order difference operator, respectively. For second-order derivatives, D_{xx}, D_{yy} correspond to the respective second-order central difference operators. The pressure gradient will be approximated with a first-order forward difference operator, whereas the terms with velocity will be approximated by a second-order central difference operator. Thus, if $\nabla_{[n]}$ and $\nabla^2_{[2]}$ denote the discrete gradient and Laplacian, respectively, we have from the momentum equation (1) semi-discrete approximation

$$\frac{\partial \mathbf{u}_{i,j}}{\partial t} = -\nabla_{[1]} P_{i,j} - \mathbf{u}_{i,j}.\nabla_{[2]}\mathbf{u}_{i,j} + \frac{1}{Re}\nabla^2_{[2]}\mathbf{u}_{i,j} + \mathbf{F}[\mathbf{u}_{i,j}, \theta_{i,j}] \tag{17}$$

For the energy equation (3), we have the following semi-discrete approximation

$$\frac{\partial \theta_{i,j}}{\partial t} = -\mathbf{u}_{i,j}\cdot\nabla_{[2]}\theta_{i,j} + \frac{1}{Pe}\nabla^2_{[2]}\theta_{i,j} \tag{18}$$

At the boundary, the gradients and Laplacians for the velocity and energy fields are approximated with second-order precision. This allows to have a second-order scheme through the closed domain $\overline{\Omega}$. Also, to improve the numerical stability when computing the pressure from the Poisson equation.

3.1. Time discretization

There are many available methods for time discretization. In order to reduce the computational cost, the explicit first-order Euler method will be employed. Thus, from Equation (17) we have the time approximation scheme

$$\frac{\mathbf{u}^{k+1}_{i,j} - \mathbf{u}^{k}_{i,j}}{\Delta t} = -\nabla_{[1]} P^k_{i,j} + \mathbf{U}^k_{i,j} \tag{19}$$

where

$$\mathbf{U}_{i,j} = -\mathbf{u}_{i,j}\cdot\nabla_{[2]}\mathbf{u}_{i,j} + \frac{1}{Re}\nabla^2_{[2]}\mathbf{u}_{i,j} + \mathbf{F}[\mathbf{u}_{i,j}, \theta_{i,j}] \tag{20}$$

Copyright © 2008 John Wiley & Sons, Ltd.

DOI: 10.1002/fld

In an analogous way, from Equation (18), we have the time approximation scheme for the energy equation

$$\frac{\theta_{i,j}^{k+1}-\theta_{i,j}^{k}}{\Delta t}=-\mathbf{u}_{i,j}\cdot\nabla_{[2]}\theta_{i,j}^{k}+\frac{1}{Re}\nabla_{[2]}^{2}\theta_{i,j}^{k}$$
$$i=1:N,\quad j=1:M,\quad k=0,1,\ldots \tag{21}$$

4. DISCRETIZATION OF THE POISSON EQUATION FOR THE PRESSURE

The discretization of the Poisson equation for the pressure of incompressible flows requires special attention. It is required that the solution of Equation (19) satisfies the continuity equation in the interior of the spatial region Ω.

Since the pressure field to be calculated is time-dependent, the discretization of the equation for the pressure (14) is performed for an arbitrary but fixed time. This is done in conjunction with the Neumann condition (15) at the boundary Γ.

The pressure field is determined up to an additive constant corresponding to the level of the hydrostatic pressure. This can be removed by prescribing the integral relationship $c=\iint_{\Omega}P(x,y)\,\mathrm{d}x\,\mathrm{d}y$, or by a grounding condition at certain point $P(x_0,y_0)=0$. This later condition will be considered. Thus, for a given discrete solution $P_{i,j}$, although $(P_{i,j}+c)$ is also a solution for any constant c, the grounding condition allow us to determine the pressure by choosing $c=0$.

By taking divergence in Equation (19), and to keep valid the continuity equation at level time $(k+1)$, it follows that

$$\nabla^{2}P^{k}=\frac{\nabla\cdot\mathbf{u}^{k}}{\Delta t}+\nabla\cdot f(\mathbf{u}^{k}) \tag{22}$$

where f contains all viscous and convective terms as well as the rotating term $\mathbf{F}$. By applying a second-order central difference approximation on a staggered grid, the Poisson equation (22) becomes

$$\nabla_{[2]}^{2}P_{i,j}=\nabla_{[1]}\cdot\mathbf{U}_{i,j}+D_t \tag{23}$$

where $\mathbf{U}_{i,j}$ is as given in (20). Here the term $D_t=\nabla.\mathbf{u}^{k}/\Delta t$ corresponds to dilatation and it is maintained with the purpose of eliminating non-linear instabilities [19–21].

On the other hand, the continuity Equation (2) discretized at the level time $(k+1)$ must be satisfied exactly, that is

$$0=D_{1x}u_{i-1,j}^{k+1}+D_{1y}v_{i,j-1}^{k+1} \tag{24}$$

Dividing Equation (24) by Δt, we have the dilatation term

$$0=\frac{D_{1x}u_{i-1,j}^{k+1}+D_{1y}v_{i,j-1}^{k+1}}{\Delta t}=D_t^{k+1} \tag{25}$$

Substituting the approximated momentum Equation (19) in Equation (25), it follows that at each level time k,

$$D_{1x}D_{1x}P_{i-1,j}+D_{1y}D_{1y}P_{i,j-1}=D_t+D_{1x}U_{i-1,j}+D_{1y}V_{i,j-1} \tag{26}$$

Copyright © 2008 John Wiley & Sons, Ltd.

DOI: 10.1002/fld

Since the involved operators satisfy $D_{1x}D_{1x}P_{i-1,j}=D_{xx}P_{i,j}$, $D_{1y}D_{1y}P_{i,j-1}=D_{yy}P_{i,j}$ it follows from Equation (26) that

$$\nabla^2_{[2]}P_{i,j}=D_{1x}U_{i-1,j}+D_{1y}V_{i,j-1}+D_t,\quad i=1:N,\quad j=1:M \tag{27}$$

This is the discretized Poisson equation at level time k.

In order to have good convergence of the approximate solution of (23), the compatibility condition (16) should be satisfied exactly in the discrete form, that is [22, 23],

$$\sum_{i,j\in\Omega}\nabla^2 P_{i,j}=\sum_{i,j\in\Gamma}\frac{\partial P_{i,j}}{\partial n}$$

In fact, by considering $\Delta x=\Delta y=h$ in Equation (27), we have

$$\begin{aligned}&\sum_{i,j=1}^{N,M}(P_{i,j-1}+P_{i-1,j}-4P_{i,j}+P_{i+1,j}+P_{i,j+1})\\&\quad=h^2\sum_{i,j=1}^{N,M}D_t+h\sum_{i,j=1}^{N,M}(U_{i,j}-U_{i-1,j}+V_{i,j}-V_{i,j-1})\end{aligned} \tag{28}$$

It turns out that

$$\begin{aligned}&\sum_{i=1}^{N}(P_{i,0}-P_{i,1}+P_{i,M+1}-P_{i,M})+\sum_{j=1}^{M}(P_{0,j}-P_{1,j}+P_{N+1,j}-P_{N,j})\\&\quad=h\sum_{i=1}^{N}(V_{i,M}-V_{i,0})+\sum_{j=1}^{M}(U_{N,j}-U_{0,j})\end{aligned} \tag{29}$$

From the above equation, the discrete Neumann conditions should satisfy the four following relationships:

$$P_{0,j}=P_{1,j}-hU_{0,j},\quad j=1,\ldots,M \tag{30}$$

$$P_{N+1,j}=P_{N,j}+hU_{N,j},\quad j=1,\ldots,M \tag{31}$$

$$P_{i,0}=P_{i,1}-hV_{i,0},\quad i=1,\ldots,N \tag{32}$$

$$P_{i,M+1}=P_{i,M}-hV_{i,M},\quad i=1,\ldots,N \tag{33}$$

Let us observe that these conditions are a discrete version of Equation (15).

5. A PRESSURE–VELOCITY ALGORITHM

We shall follow an algorithm introduced by Claeyssen *et al.* [1]. At each time level, the pressure is updated in one step and then the velocity field is calculated. The pressure is initialized by solving a singular system that appears from the discretization of the Poisson equation with a Neumann condition. When solving the Poisson equation, a special treatment is given to the interior points that correspond to the interior cells and to the adjacent cells, in such a way that the compatibility condition is verified. This actualization contains correction terms for a direct computing of the

Copyright © 2008 John Wiley & Sons, Ltd.

DOI: 10.1002/fld

pressure at the interior points of the interior cells. This is done by incorporating the values of the pressure already calculated in neighboring points. This procedure is described as follows.

Let $\mathbf{u}=\mathbf{u}_{i,j}$ and $P=P_{i,j}$. The pressure is initialized by solving the equation

$$\nabla^2_{[2]}P=D_t+\nabla_{[1]}.\left(-\mathbf{u}^k.\nabla_{[2]}\mathbf{u}^k+\frac{1}{Re}\nabla^2_{[2]}\mathbf{u}^k\right) \tag{34}$$

with a SOR method for $k=0$ [1].

For a direct update of the variables, Equation (17) is used.

Let us assume that all discrete variables are known at the time k. We consider $\mathbf{v}^*$ as the velocity that would appear as the solution of Equation (17) with an absent pressure gradient by knowing the field $\mathbf{u}^k$, that is

$$\frac{\mathbf{v}^*-\mathbf{u}^k}{\Delta t_1}=-\mathbf{u}^k\cdot\nabla_{[2]}\mathbf{u}^k+\frac{1}{Re}\nabla^2_{[2]}\mathbf{u}^k+\mathbf{F}[\mathbf{u}^k,\theta^k] \tag{35}$$

Thus

$$\mathbf{v}^*=\mathbf{u}^k+\Delta t_1\left(-\mathbf{u}^k\cdot\nabla_{[2]}\mathbf{u}^k+\frac{1}{Re}\nabla^2_{[2]}\mathbf{u}^k+\mathbf{F}[\mathbf{u}^k,\theta^k]\right) \tag{36}$$

The variable $\mathbf{v}^*$ is known as *pseudo-velocity* [9], and does not necessarily satisfy the continuity equation. The Helmholtz theorem [24, 25] allows $\mathbf{v}^*$ to be expressed as

$$\mathbf{v}^*=r\nabla P^{k+1}+A \quad \text{such that } \nabla\cdot A=0 \tag{37}$$

Now, defining the velocity at time $(k+1)$ as $\mathbf{u}^{k+1}=A$, and the step of time as $\Delta t=r$, it follows, by using (36), the discrete version of (17), with $\Delta t_1=\Delta t$,

$$\frac{\mathbf{u}^{k+1}-\mathbf{u}^k}{\Delta t}=-\nabla_{[1]}P^{k+1}-\mathbf{u}^k.\nabla_{[2]}\mathbf{u}^k+\frac{1}{Re}\nabla^2_{[2]}\mathbf{u}^k+\mathbf{F}[\mathbf{u}^k,\theta^k] \tag{38}$$

Thus, $\mathbf{u}^{k+1}$ is a discrete solution of Equation (17) and satisfies the continuity equation.

Now, by taking divergence in (38), we arrive at the following discrete equation for the pressure at the level time $(k+1)$,

$$\begin{aligned}\nabla^2_{[2]}P^{k+1}&=\frac{\nabla.\mathbf{v}^k}{\Delta t}+\nabla_{[1]}\cdot\left(-\mathbf{u}^k\cdot\nabla_{[2]}\mathbf{u}^k+\frac{1}{Re}\nabla^2_{[2]}\mathbf{u}^k+\mathbf{F}[\mathbf{u}^k,\theta^k]\right)\\&=\nabla\cdot\mathbf{U}^k+D_t^k\end{aligned} \tag{39}$$

The fictitious values that appear in the discretization of the Neumann condition (30)–(33), are calculated through the following equations:

$$P^{k+1}_{0,j}=P^k_{1,j}-hU^k_{0,j},\quad j=1,\ldots,M \tag{40}$$

$$P^{k+1}_{N-1,j}=P^k_{N,j}+hU^k_{N,j},\quad j=1,\ldots,M \tag{41}$$

$$P^{k+1}_{i,0}=P^k_{i,1}-hV^k_{i,0},\quad i=1,\ldots,N \tag{42}$$

$$P^{k+1}_{i,M+1}=P^k_{i,M}-hV^k_{i,M},\quad i=1,\ldots,N \tag{43}$$

Copyright © 2008 John Wiley & Sons, Ltd.

DOI: 10.1002/fld

For the interior points, the pressure field is up-dated by solving Equation (39) with the incorporation of values already determined, that is, we consider the one-step scheme for computing the pressure field

$$P_{i,j}^{k+1}=\tfrac{1}{4}(P_{i,j-1}^{k+1}+P_{i-1,j}^{k+1}+P_{i+1,j}^{k}+P_{i,j+1}^{k}+h^2\nabla_{[1]}\mathbf{U}^k+h^2D_t^k) \tag{44}$$

where $\Delta x=\Delta y=h$.

5.1. The pressure–velocity algorithm

With the above discussion, an algorithm for integrating the Navier–Stokes equations for a rotating flow with a prescribed Neumann condition for the pressure can be formulated as follows.

1. Introduction of the initial velocity, corresponding to the initial time level $k=0$, the boundary conditions and involved physical parameters.
2. Initialization of the pressure through Equation (34).
3. Calculation of the pseudo-velocity field v^* by using (36).
4. One step updating of the pressure field by using (40)–(44).
5. Update the temperature field θ^{k+1} through (21).
6. Update of the velocity field $\mathbf{u}^{k+1}$ through (38).
7. To do steps (3)–(6) for $k=1,2,\ldots$.
8. End the calculations.

6. ROTATING WEAKLY VISCOELASTIC FLOW

The model considered in this work appears in turbomachinery where we can suppose that a substance through spinning can be dissolved to form a solution. It is assumed that a small amount of polymer added to a Newtonian liquid can create a highly diluted viscoelastic fluid, which can be considerably more stable in the presence of rotations. The prediction of the behavior requires adoption of appropriate constitutive equations and rheological parameters. Constitutive equations can be formulated for viscoelastic fluids in terms of the mechanical Maxwell models. The rheological behavior of a viscoelastic fluid can be simulated by a Hookean spring in series with a Newtonian viscous dashpot [26]. We shall refer to Joseph [27] for the derivation of the following constitutive equation:

$$\sigma=-p\mathbf{1}+\tau \tag{45}$$

$$\lambda\frac{\mathrm{D}\tau}{\mathrm{D}t}+\tau=2\mu\mathbf{D}[u] \tag{46}$$

Here $\sigma(t,\mathbf{x})$ is a symmetric tensor field, $\mathbf{v}(t,x)$ is a solenoidal field, τ is the so-called extra tensor and p is the reaction pressure. The type of invariant derivative that is chosen for $\mathrm{D}/\mathrm{D}t$ determines the form of constitutive equation. Thus, there are a great variety of possibilities for this (see [27, p. 80]). In this work we shall use the covariant convected derivative or *subconvective* derivative $\mathrm{D}\tau/\mathrm{D}t=\boldsymbol{\tau}^o$ with

$$\tau^o=\frac{\mathrm{d}\tau}{\mathrm{d}t}+\tau\mathbf{L}+\mathbf{L}^{\mathrm{T}}\tau \tag{47}$$

Copyright © 2008 John Wiley & Sons, Ltd.

DOI: 10.1002/fld

where **L** is the velocity gradient. In terms of components

$$\tau_{kl}^{o} = \frac{\partial \tau_{kl}}{\partial t} + \mathbf{v}\cdot\nabla\tau_{kl} + \tau_{km}\frac{\partial v_m}{\partial x_l} + \tau_{lm}\frac{\partial v_m}{\partial x_k} \tag{48}$$

For a fully developed flow with the above viscoelastic fluid and for which the physical variables are axially independent, the tensor components of a Maxwell viscoelastic flow are simplified.

We assume that the relaxation time λ of the weakly viscoelastic fluid is small and that the secondary flow is relatively weak, that is

$$\frac{\lambda v}{D^2} \ll 1, \quad \frac{U}{W} \ll 1, \quad \frac{V}{W} \ll 1 \tag{$*$}$$

where U, V, W are maximum values for the components of the velocity field and D is the length scale.

The fact of having a highly diluted fluid, suggests that the specific mass ρ and the kinematic viscosity $v = \mu/\rho$ will be the same ones as the Newtonian fluid, from which they are obtained.

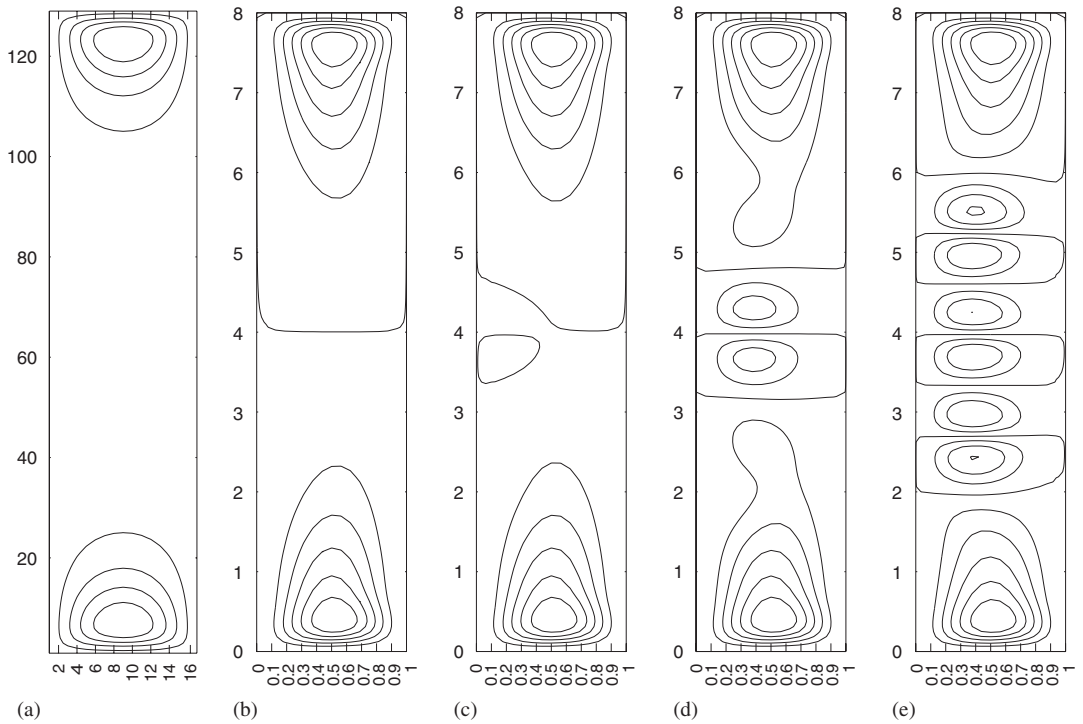

Figure 2. Streamlines of the secondary flow in a duct with aspect ratio 8:1; for t: (a) 10 s; (b) 500 s; (c) 1000 s; (d) 1600 s; and (e) fully developed, for $Re = 248$, $C = 0.057$ ($G = 2 \times 10^{-4}$ lb/ft^3), $Ro = 21.3$ ($\omega = 0.005$ rad/s), $We = 4.2969 \times 10^{-5}$.

Copyright © 2008 John Wiley & Sons, Ltd.

DOI: 10.1002/fld

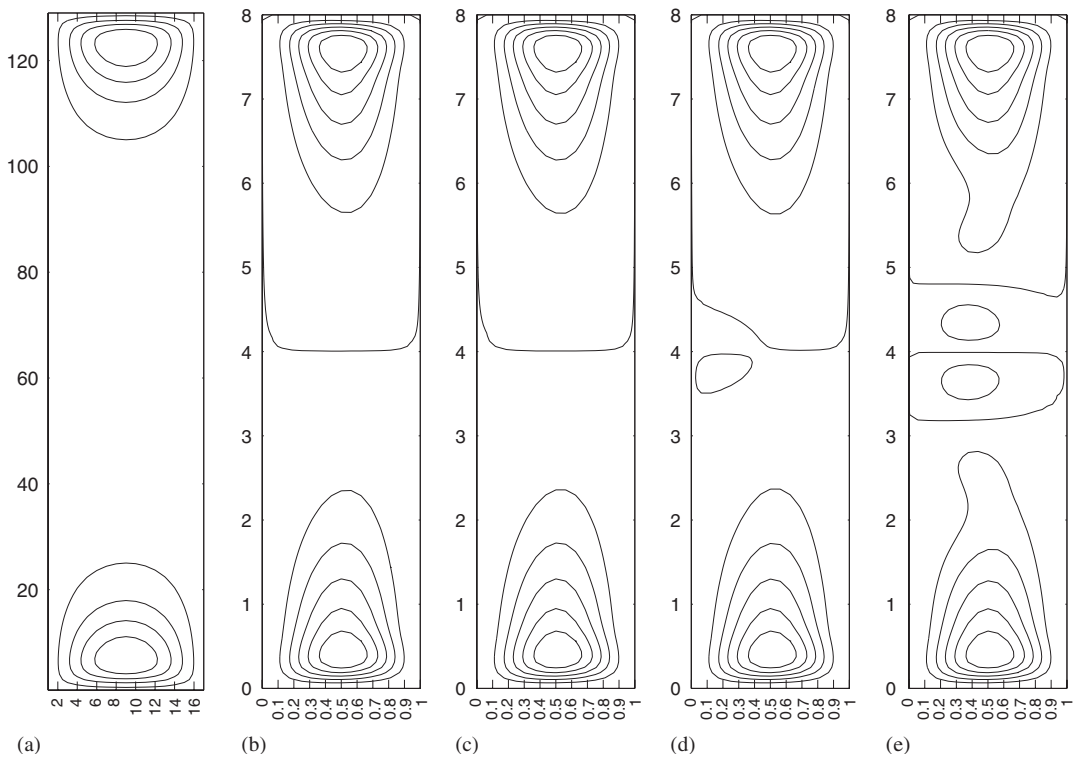

Figure 3. Streamlines of the secondary flow in a duct with aspect ratio 8:1; for t: (a) 10 s; (b) 500 s; (c) 1000 s; (d) 1600 s; and (e) fully developed, for $Re=248$, $C=0.057$ ($G=2\times10^{-4}\,\mathrm{lb/ft^3}$), $Ro=21.3$ ($\omega=0.005\,\mathrm{rad/s}$), $We=1.289\times10^{-4}$.

The hypothesis (*), implies after an order approximation analysis, that the components of the dissipative stress tensor can be approximate for the following equations:

$$\tau_{zz}=0$$

and

$$\tau_{xx}+2\lambda\tau_{xz}\frac{\partial w}{\partial x}=2\mu\frac{\partial u}{\partial x}$$

$$\tau_{xy}+\lambda\left(\tau_{xz}\frac{\partial w}{\partial y}+\tau_{yz}\frac{\partial w}{\partial x}\right)=\mu\left(\frac{\partial u}{\partial y}+\frac{\partial v}{\partial x}\right)$$

$$\tau_{xz}+\lambda\tau_{zz}\frac{\partial w}{\partial x}=\mu\frac{\partial w}{\partial x}$$

Copyright © 2008 John Wiley & Sons, Ltd.

DOI: 10.1002/fld

$$\tau_{yy}+\lambda\tau_{yz}\frac{\partial w}{\partial y}=2\mu\frac{\partial v}{\partial y}$$

$$\tau_{yz}+\lambda\tau_{zz}\frac{\partial w}{\partial y}=\mu\frac{\partial w}{\partial y}$$

Denoting by $\nu=\mu/\rho$ the kinematic viscosity, $(\nabla w)^2=(\partial w/\partial x)^2+(\partial w/\partial y)^2$ the value of the longitudinal velocity gradient, using the continuity equation and by substituting in the balance momentum equation

$$\rho\left[\frac{\partial \mathbf{v}}{\partial t}+\mathbf{v}\cdot\nabla\mathbf{v}+2\boldsymbol{\omega}\times\mathbf{v}\right]=-\nabla p+\nabla\cdot\tau$$

we have

$$\frac{\partial u}{\partial t}+u\frac{\partial u}{\partial x}+v\frac{\partial u}{\partial y}=-\frac{1}{\rho}\frac{\partial p}{\partial x}+\nu\nabla^2 u-2\lambda\nu\left(\frac{\partial w}{\partial x}\nabla^2 w+\frac{1}{2}\frac{\partial}{\partial x}(\nabla w)^2\right)-2\omega w$$

$$\frac{\partial v}{\partial t}+u\frac{\partial v}{\partial x}+v\frac{\partial v}{\partial y}=-\frac{1}{\rho}\frac{\partial p}{\partial y}+\nu\nabla^2 v-2\lambda\nu\left(\frac{\partial w}{\partial y}\nabla^2 w+\frac{1}{2}\frac{\partial}{\partial y}(\nabla w)^2\right)$$

$$\frac{\partial w}{\partial t}+u\frac{\partial w}{\partial x}+v\frac{\partial w}{\partial y}=-\frac{1}{\rho}\frac{\partial p}{\partial z}+\nu\nabla^2 w+2\omega u$$

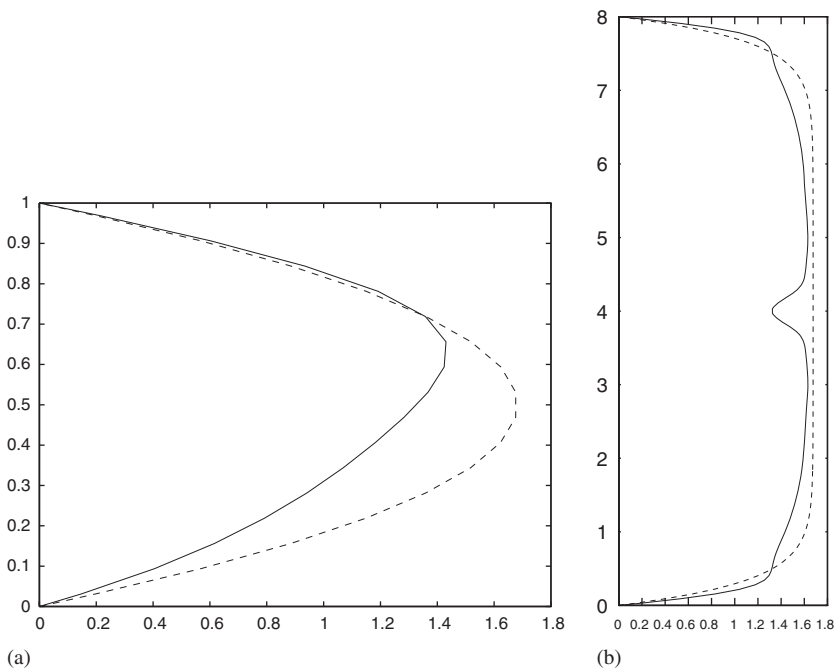

Figure 4. Axial velocity profiles in a duct 8:1; $Re=248$, $C=0.057$, $Ro=21.3$: (a) horizontal and (b) vertical, dashed lines for $\lambda=0$ and continuous lines for $\lambda=0.3$, $We=1.289\times10^{-4}$, $Q_f/Q=0.9654$.

Copyright © 2008 John Wiley & Sons, Ltd.

DOI: 10.1002/fld

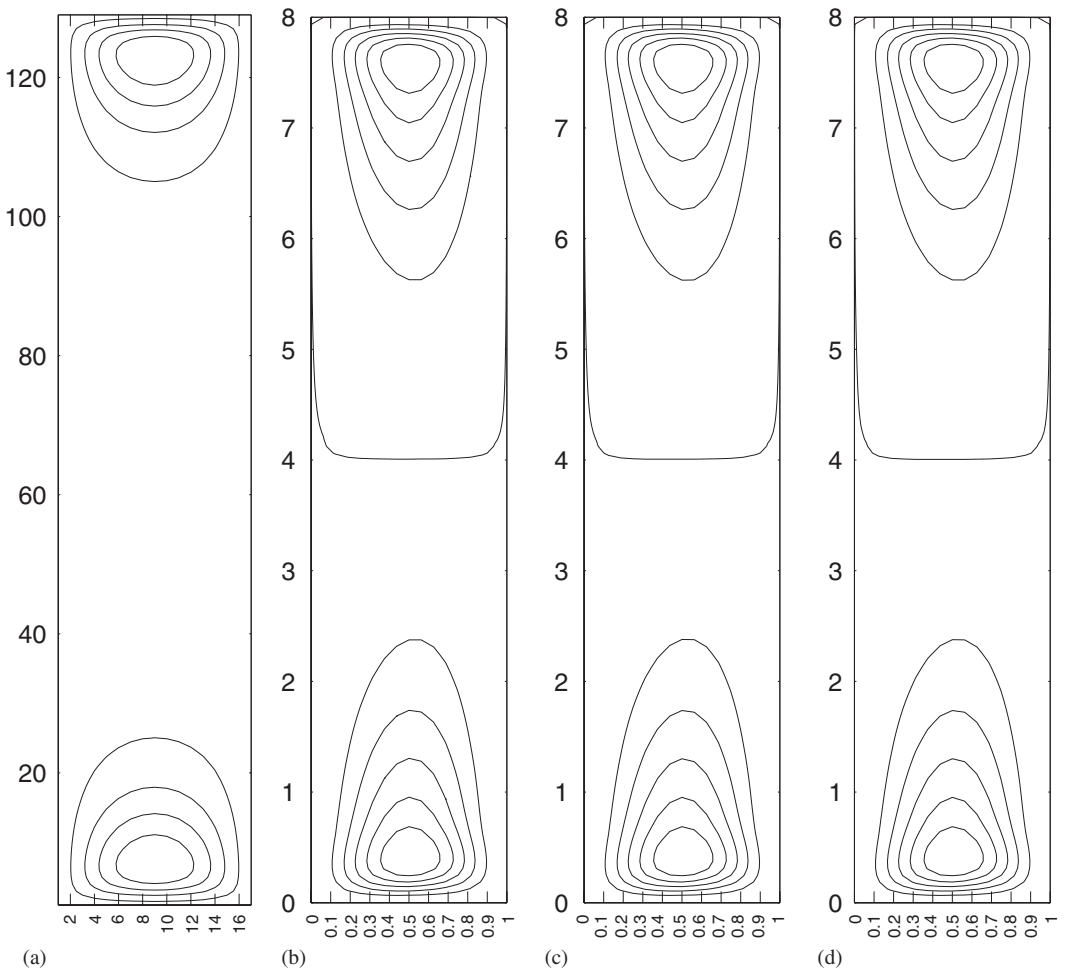

Figure 5. Streamlines of the secondary flow in a duct with aspect ratio 8:1; for t: (a) 10 s; (b) 500 s; (c) 1600 s; and (d) fully developed, for $Re=248$, $C=0.057$ ($G=2\times10^{-4}\,\mathrm{lb/ft^3}$), $Ro=21.3$ ($\omega=0.005\,\mathrm{rad/s}$), $We=2.1484\times10^{-4}$.

On the basis of the above assumptions and in dimensionless form, we obtain the following model:

$$\frac{\partial \mathbf{u}}{\partial t}+\mathbf{u}\cdot\nabla\mathbf{u}+\nabla P=\frac{1}{Re}\nabla^2\mathbf{u}+\mathbf{F}(\mathbf{u}) \quad \text{in } \Omega,\ \ t>0 \tag{49}$$

$$\nabla\cdot\mathbf{u}=0 \quad \text{in } \Omega\ \ t>0 \tag{50}$$

$$\begin{aligned}\mathbf{u}&=(u(t,x,y),v(t,x,y),w(t,x,y))\\ \mathbf{F}(\mathbf{u})&=(2/Ro)\mathbf{j}\times\mathbf{u}-2We(\nabla^2 w\nabla w+\tfrac{1}{2}\nabla(\nabla w)^2)\end{aligned} \tag{51}$$

Copyright © 2008 John Wiley & Sons, Ltd.

DOI: 10.1002/fld

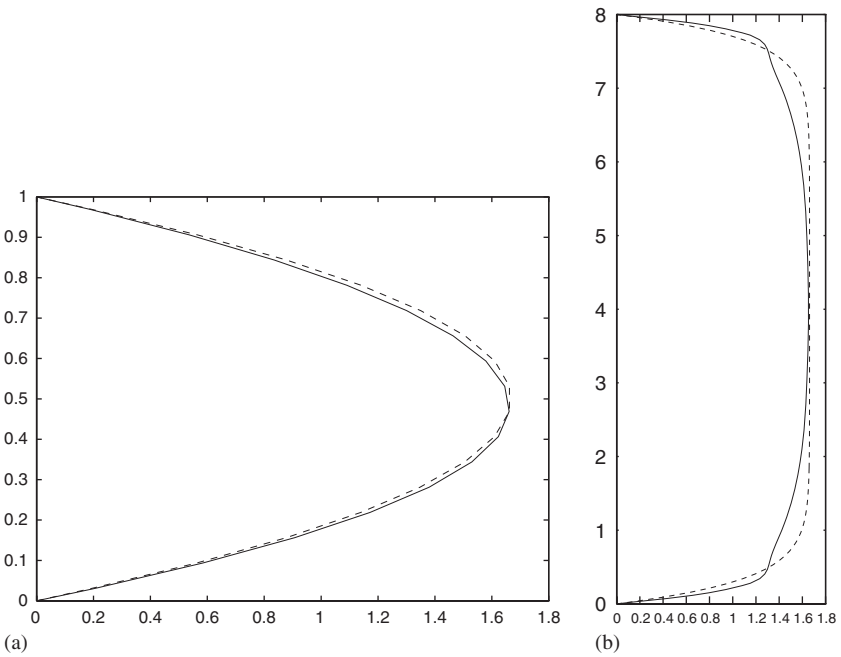

Figure 6. Axial velocity profiles in a duct 8:1; $Re=248$, $C=0.057$, $Ro=21.3$: (a) horizontal and (b) vertical, with dashed lines for $\lambda=0$ and continuous lines for $\lambda=0.5$, $We=2.1484\times10^{-4}$, $Q_f/Q=0.9735$.

that will be employed for determining the secondary flow in a transversal section $(0,D)\times(0,H)$ perpendicular to the axis of the duct as in Figure 1. The aspect ratio is given for $\chi=H/D$.

6.1. Numerical simulations

Here, we consider the results of the numerical simulations for a rotating weakly viscoelastic fluid in a duct by using the direct velocity–pressure algorithm given before with a Neumann condition for the pressure. The objective is to examine the effects of rotation on the secondary flow in ducts with aspect ratio 8:1 and 2:1. In the first case, a uniform grid of 16×128 points was considered, where $\Delta x=\Delta y=0.01$ ft. For the duct of ratio 2:1, a grid of 32×64 points was used, where $\Delta x=\Delta y=0.005$ ft. The results were accomplished by choosing a time step $\Delta t=0.001$ in order to arrive quickly at the fully developed flow. This time step value satisfies the classical linear stability condition [5, 19]. Through numerical experiments, on a series of refined grids, we obtained that the solution converged to a grid-independent solution. Two basic facts contributed for this. The spatial scheme, including the discretization at the boundary, turned out to be of second-order. The one step update, besides the discrete compatibility of the pressure Neumann condition, introduces a filtering that is useful for obtaining a desired numerical convergence.

We consider the initial velocity field conditions $u(0)=v(0)=0$ and $w(0)=w_1$, where w_1 is determined by solving the Poisson equation

$$-\Delta w_1=Re\,C \tag{52}$$

Copyright © 2008 John Wiley & Sons, Ltd.

DOI: 10.1002/fld

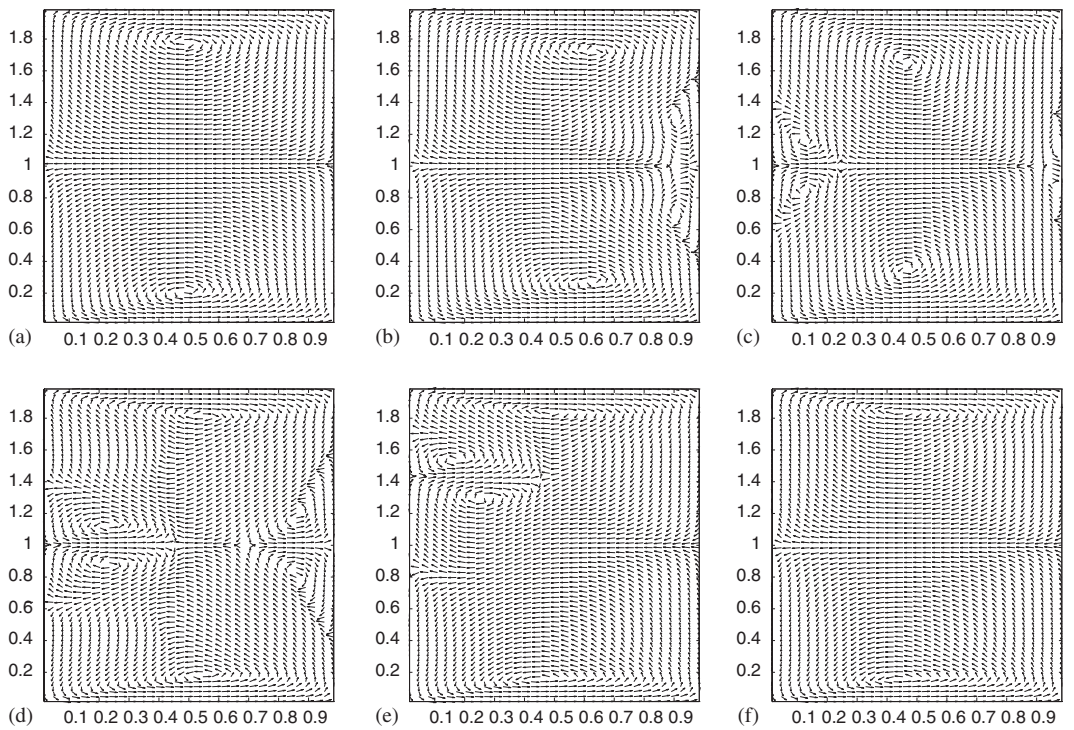

Figure 7. Secondary flow in a duct 2:1; t: (a) 1 s; (b) 12.5 s; (c) 40 s; (d) 75 s; (e) 400 s; and (f) fully developed, for $Re=279$, $C=0.1345$ ($G=6\times10^{-4}\,\mathrm{lb/ft^3}$), $Ro=1.198$ ($\omega=0, 1\,\mathrm{rad/s}$), $We=1.289\times10^{-4}$.

subject to a non-slip boundary condition $w=0$ on Γ. Thus, w_1 corresponds to a classical quasi-parabolic profile. At the walls of the duct, were prescribed the conditions $u=0, v=0, w=0$.

Speziale [5] mentions a qualitative comparison of this type of secondary flow with a Newtonian structure when the Weissenberg number is included. However, he does not exhibit greater results about the structure of this flow for weakly viscoelastic fluids. It is left as a proposal for future studies. In this work we shall exhibit the flow mentioned by Speziale.

In the case of aspect ratio 8:1, simulations were carried out for three physical situations obtained by a variation of the Weissenberg number, while keeping fixed the other bulk properties of the fluid such as specific mass $\rho=1.936\,\mathrm{slugs/ft^3}$ and viscosity $v=1.1\times10^{-5}\,\mathrm{ft^2/s}$, corresponding to water at an environment mean temperature. The longitudinal pressure gradient is kept constant at $G=2\times10^{-4}\,\mathrm{lb/ft^3}$. For a weak rotation, it is considered the angular velocity $\omega=0.005\,\mathrm{rad/s}$. These later parameters correspond to the flow of a Newtonian fluid [4, 28]. They will be compared with the structure of a weak rotating viscoelastic fluid by controlling the Weissenberg number.

In the first situation, we chose $We=4.2969\times10^{-5}$, that corresponds to the relaxation time of $\lambda=0.1(\mathrm{s})$. The secondary flow is shown for different times in Figure 2. It can be observed that the secondary flow develops slower than in the case of a Newtonian flow [4, 28], until it reaches a fully developed state in approximately $t=4000\,\mathrm{s}$.

Copyright © 2008 John Wiley & Sons, Ltd.

DOI: 10.1002/fld

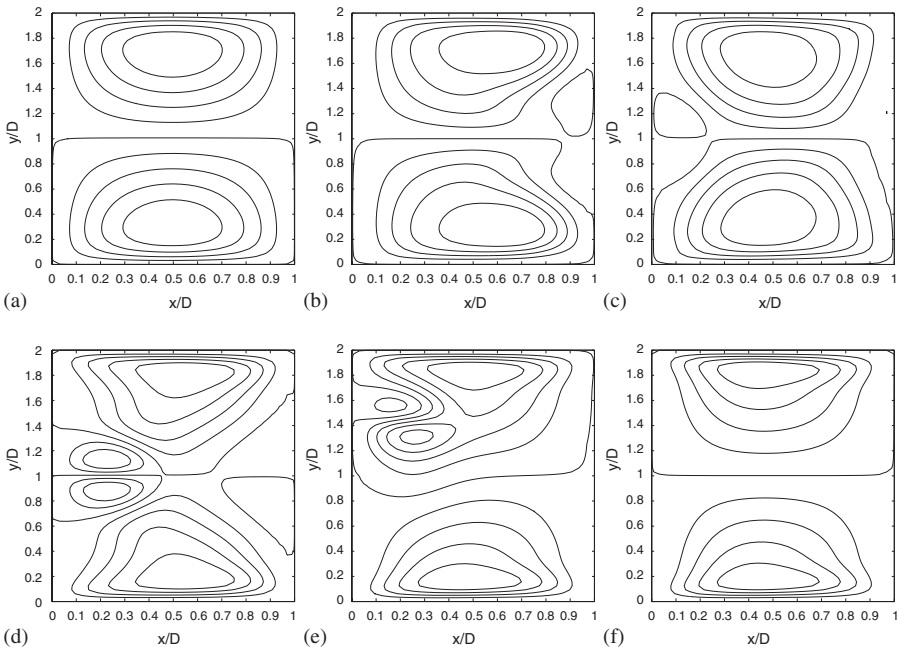

Figure 8. Streamlines of the secondary flow in a duct with aspect ratio 2:1, for t: (a) 1 s; (b) 12.5 s; (c) 40 s; (d) 75 s; (e) 400 s; and (f) fully developed, for $Re=279$, $C=0.1345$ ($G=6\times10^{-4}\,\mathrm{lb/ft^3}$), $Ro=1.198$ ($\omega=0.1\,\mathrm{rad/s}$), $We=1.289\times10^{-4}$.

In Figure 3 is shown the streamlines of the velocity field for $We=1.289\times10^{-4}$ ($\lambda=0.3$). It is observed that the secondary flow tends to stabilize with only two vortexes, in the center of the transversal section. The vortexes begin to appear in approximately $t=1600$ s, reaching the stationary state in approximately $t=3000$ s. This structure differs from the previous case, where six vortexes are developed.

The longitudinal velocity profiles, fully developed, in the central lines of the transversal section of the duct, for $We=1.289\times10^{-4}$, are shown in Figure 4. The horizontal profile is for $y/D=4$ and vertical one for $x/D=0.5$. It can be observed that the appearance of two vortexes in the center of the duct, generates a deviation of the horizontal profile in the direction of the side $x/D=1$. However, the flowrate is reduced with a change rate of approximately 3.5% in relation to the flowrate of the longitudinal flow. The profiles, for $We=4.2969\times10^{-5}$, have a very similar behavior to the Newtonian case [4, 28] and they are not shown here.

With a further increase of the viscoelastic coefficient, say $We=2.1484\times10^{-4}$ ($\lambda=0.5$), we are able to stabilize the secondary flow with a structure of two vortexes at the ends, as can be observed in Figure 5. The fully developed state is reached in approximately $t=600$ s, a much smaller time in relation to the other preceding cases. This state is commented on by Speziale [5], without presenting results, saying that for a larger Weissenberg number, satisfying $We>7.4\times10^{-5}$, the flow structure stabilizes with two vortexes.

The longitudinal velocity profiles, at the central lines of the transversal section of the duct, are exhibited in Figure 6 for $We=2.1484\times10^{-4}$ with a flowrate of approximately 2.7% in the longitudinal direction. It is observed that when the Weissenberg number increases, the secondary

Copyright © 2008 John Wiley & Sons, Ltd.

DOI: 10.1002/fld

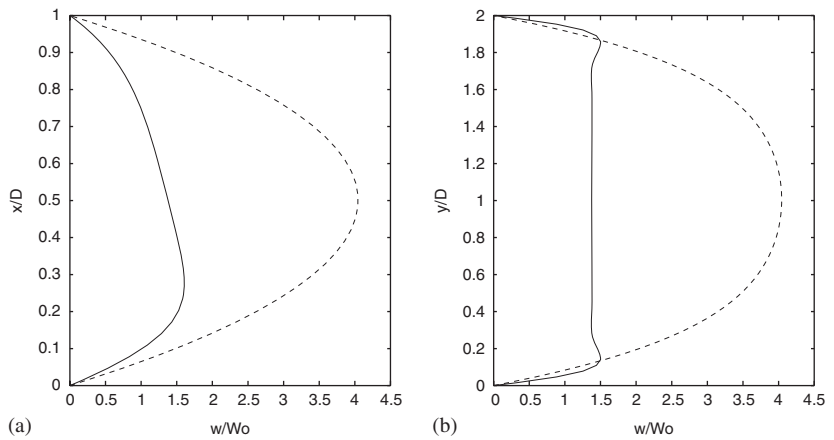

Figure 9. Axial velocity profiles in a duct 2:1, $Re=279$, $Ro=1.198$, $We=1.289\times10^{-4}$: (a) horizontal and (b) vertical [dashed line ($\omega=0$), continuous line ($\omega=0.1\,\mathrm{rad/s}$)]. $Q_f/Q=0.5125$, $u_{\max}/w_{\max}=0.128$.

flows of a dilute, weakly viscoelastic fluid generate a reduction in the loss of the flowrate in the longitudinal direction, as shown in Figures 4 and 6, in comparison to the reduction of 7%, that happens in the case of a Newtonian fluid [4, 28].

In Figures 7 and 8, are shown the velocity fields and streamlines of the secondary flow, in a duct with a aspect ratio 2:1, for $We=1.289\times10^{-4}$, with angular velocity $\omega=0.1\,\mathrm{rad/s}$, and a longitudinal velocity gradient $G=6\times10^{-4}\,\mathrm{lb/ft^3}$. It is observed that for weakly viscoelastic fluids, besides the two main vortexes, there appear two secondary vortexes in the medium section of the duct (Figure 8(d)). The secondary vortexes are dissipated and after a certain period of instability, the flow is able to stabilize in two counter-rotating vortexes.

The longitudinal velocity profiles can be seen in Figure 9, where the flowrate, due to the effects of this secondary flow, is of 48.6% relative to the flowrate without rotation.

7. MIXED CONVECTION WITH A ROTATION WEAKLY VISCOELASTIC FLOW

The stability of a convective fluid movement, where it exists with a difference of temperature in the vertical side walls, with high aspect ratio, is studied numerically. For the problem of a weakly viscoelastic fluid the flow considered is one of mixed convection, in the interior of the duct in rotation. This later phenomena appears in engineering applications such as in cooling systems for conductors of electric generators, separation processes, rotating heat exchangers and turbomachinery.

The problem is generated by the heating of one of the walls of the rectangular section with constant temperature, T_h (internal wall), while the opposite wall remains cold with temperature T_c ($T_c<T_h$), and the horizontal walls are kept adiabatic, as shown in Figure 1.

A convective flow is generated by the buoyancy forces as soon as the left vertical wall temperature is increased to a constant value, while the right vertical wall is kept at a lower temperature. Here we assume that the flow is laminar and the fluid inside of the duct is weakly viscoelastic. It is also considered that the Boussinesq approximation is valid, which imply that the fluid properties,

Copyright © 2008 John Wiley & Sons, Ltd.

DOI: 10.1002/fld

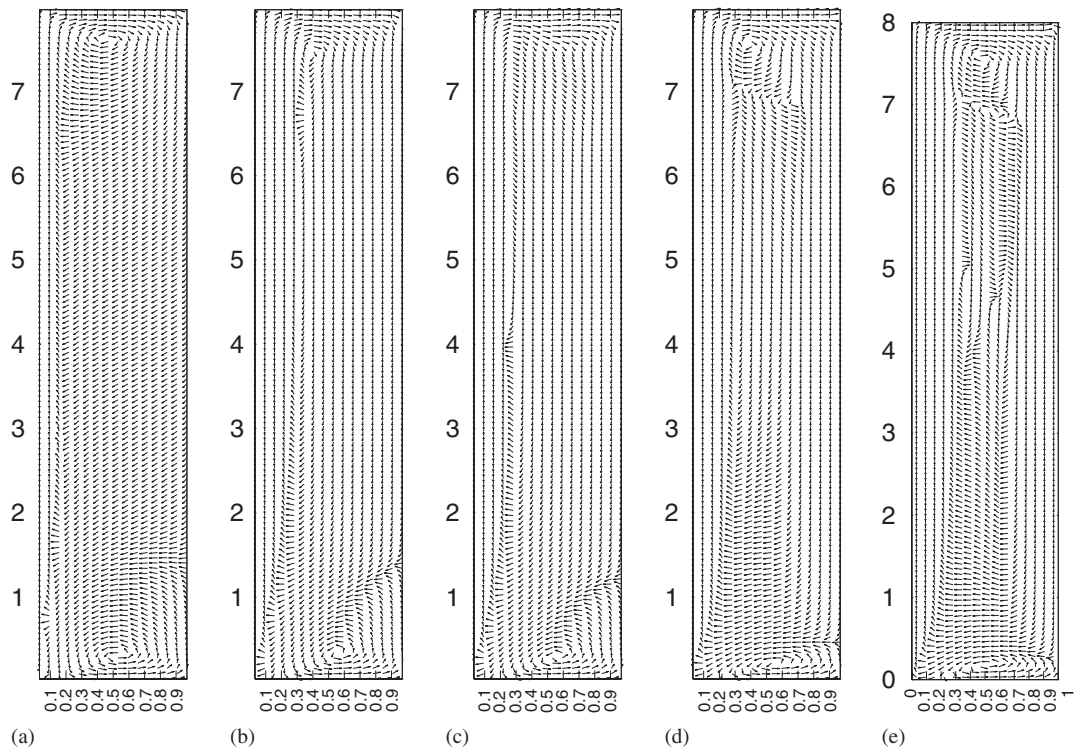

Figure 10. Secondary flow in a duct 8:1; for t: (a) 10 s; (b) 100 s; (c) 500 s; (d) 1600 s; and (e) fully developed, for $Re=260$, $C=0.057$ ($G=2\times10^{-4}$ lb/ft^3), $Ro=21.3$ ($\omega=0.005$ rad/s), $We=2.1484\times10^{-4}$, $Gr=54331$, $Pr=8$.

the coefficient of volumetric expansion β and the viscosity coefficient v, are constants and that the buoyancy term appears only in the momentum equation as a linear function of the temperature. No sources of heat will be considered in the interior.

Based on the above assumptions, the non-dimensional momentum equation that govern the flow of this problem can be expressed on the following form:

$$\frac{\partial u}{\partial t}+u\frac{\partial u}{\partial x}+v\frac{\partial u}{\partial y}=-\frac{\partial P}{\partial x}+\frac{1}{Re}\nabla^2 u$$
$$-2We\left(\frac{\partial w}{\partial x}\nabla^2 w+\frac{1}{2}\frac{\partial}{\partial x}(\nabla w)^2\right)-2\frac{1}{Ro}w \tag{53}$$

$$\frac{\partial v}{\partial t}+u\frac{\partial v}{\partial x}+v\frac{\partial v}{\partial y}=-\frac{\partial P}{\partial y}+\frac{1}{Re}\nabla^2 v$$
$$-2We\left(\frac{\partial w}{\partial y}\nabla^2 w+\frac{1}{2}\frac{\partial}{\partial y}(\nabla w)^2\right)+\frac{Gr}{Re^2}\,\theta \tag{54}$$

Copyright © 2008 John Wiley & Sons, Ltd.

DOI: 10.1002/fld

$$\frac{\partial w}{\partial t}+u\frac{\partial w}{\partial x}+v\frac{\partial w}{\partial y}=C+\frac{1}{Re}\nabla^2 w+2\frac{1}{Ro}u \tag{55}$$

where $Gr=g\beta\Delta T D^3/\nu^2$ is the Grashof number, $C=GD/\rho W_0^2$ and $Pe=W_0 D/\alpha$ the Peclet number.

We thus consider the following model

$$\frac{\partial \mathbf{u}}{\partial t}+\mathbf{u}\cdot\nabla\mathbf{u}+\nabla P=\frac{1}{Re}\nabla^2\mathbf{u}+\mathbf{F}(\mathbf{u},\theta)\quad \text{in } \Omega,\ \ t>0 \tag{56}$$

$$\nabla\cdot\mathbf{u}=0\quad \text{in } \Omega,\ \ t>0 \tag{57}$$

$$\frac{\partial\theta}{\partial t}+\mathbf{u}\cdot\nabla\theta=\frac{1}{Pe}\nabla^2\theta\quad \text{in } \Omega,\ \ t>0 \tag{58}$$

$$\begin{aligned}&\mathbf{u}=(u(t,x,y),v(t,x,y),w(t,x,y))\\ &\mathbf{F}(\mathbf{u},\theta)=(2/Ro)\mathbf{j}\times\mathbf{u}-2We(\nabla^2 w\nabla w+\tfrac{1}{2}\nabla(\nabla w)^2)+\frac{Gr}{Re^2}\theta\mathbf{j}\end{aligned} \tag{59}$$

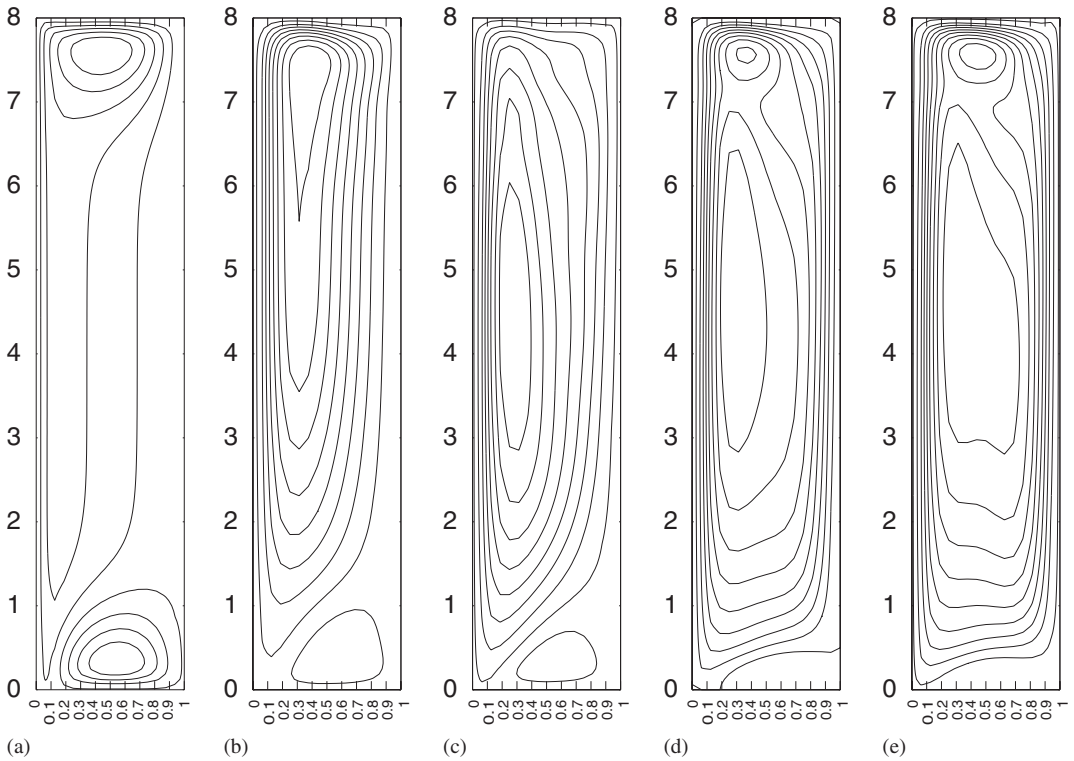

Figure 11. Streamlines of the secondary flow in a duct with aspect ratio 8:1 for t: (a) 10 s; (b) 100 s; (c) 500 s; (d) 1600 s; and (e) fully developed, for $Re=260$, $C=0.057$ ($G=2\times10^{-4}$ lb/ft^3), $Ro=21.3$ ($\omega=0.005$ rad/s), $We=2.1484\times10^{-4}$, $Gr=54\,331$, $Pr=8$.

Copyright © 2008 John Wiley & Sons, Ltd.

DOI: 10.1002/fld

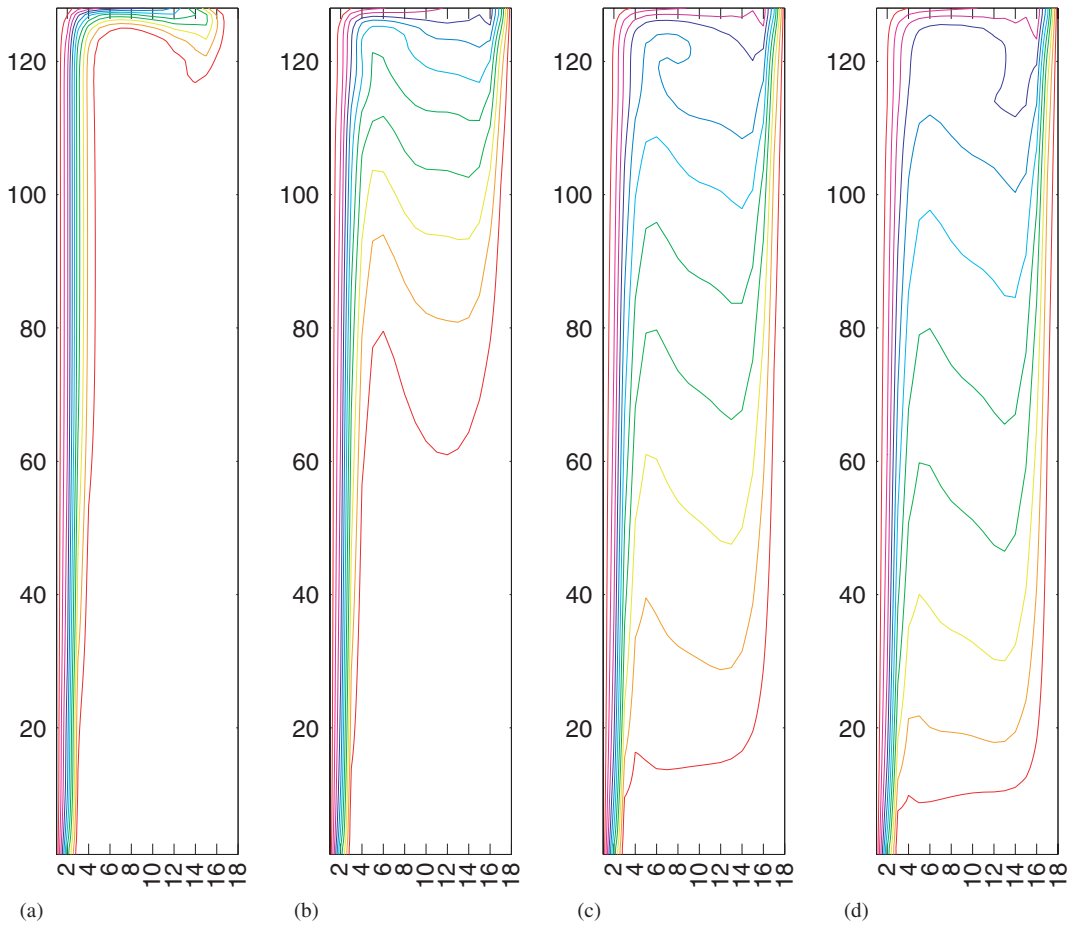

Figure 12. Isotherms for t: (a) 100 s; (b) 500 s; (c) 1600 s; and (d) fully developed, for $Re=260$, $C=0.057$ ($G=2\times10^{-4}$ lb/ft^3), $Ro=21.3$ ($\omega=0.005$ rad/s), $We=2.1484\times10^{-4}$, $Gr=54331$, $Pr=8$.

which will be employed for studying numerically the problem of mixed convection generated by the buoyancy force on a rotating weakly viscoelastic fluid.

This model is non-dimensional based on the width of the cross-section of the duct D, the side walls temperature difference $\Delta T=T_h-T_c$ and the velocity scale as the mean longitudinal velocity, fully developed W_0. We can consider also the Rayleigh number $Ra=g\beta\Delta D^3/\alpha\nu$ that relates the others numbers: $Gr/Re=Ra/Pe$.

When the above non-dimensional parameters are emphasized in the forcing term, that is, when we write $\mathbf{F}=\mathbf{F}_{(Ra,Ro,We)}$, several problems can be discussed:

- For $\beta=0$ ($Ra=0$), we have a decoupled convection problem, generated by the velocity of a rotating weakly viscoelastic flow.

Copyright © 2008 John Wiley & Sons, Ltd.

DOI: 10.1002/fld

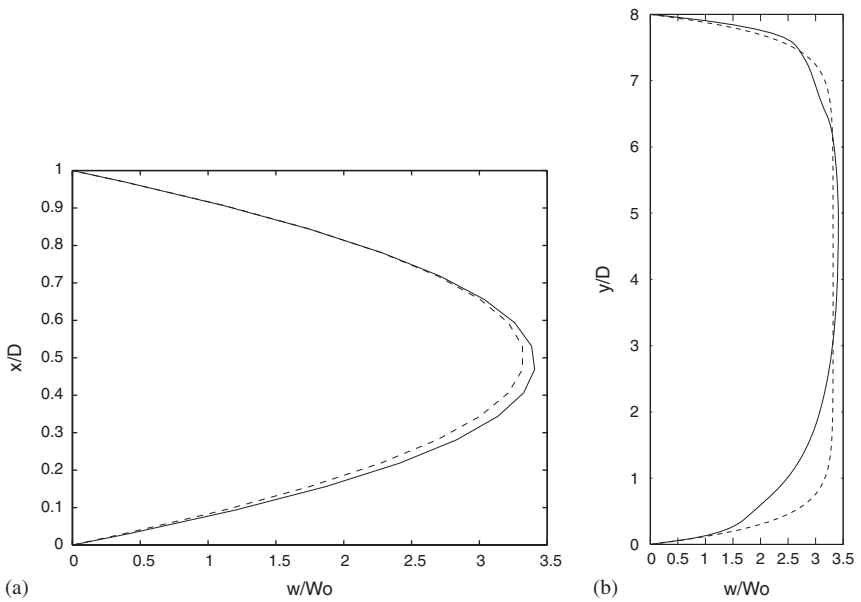

Figure 13. Axial velocity profiles: (a) horizontal and (b) vertical, for $Re=260$, $Ro=21.3$, $We=2.1484\times10^{-4}$, $Gr=54331$, $Pr=8$ [dashed line ($\omega=0$), continuous line ($\omega=0.005\,\mathrm{rad/s}$)]. $Q_f/Q=0.978$, $u_{\max}/w_{\max}=0.0456$.

- If $\beta=0$ and the elasticity coefficient $\lambda=0$ so that $Ra=0$ and $We=0$, we have a decoupled convection problem with a rotating Newtonian fluid.
- If the angular speed $\omega=0$ ($Ro=\infty$) and $Ra\neq0$, we have a natural convection problem.

Thermal properties of a fluid can be described in terms of the Prandtl number that relates viscosity with heat diffusion.

7.1. Numerical simulations

We now study numerically the problem of mixed convection generated by a buoyancy force on a rotating weakly viscoelastic fluid. The considered duct has a transversal section with aspect ratio 8:1, being the width, in a small scale $D=0.16\,\mathrm{ft}$. Other parameters that remain constant are the angular velocity $\omega=0.005\,\mathrm{rad/s}$, the longitudinal pressure gradient $G=2\times10^{-4}\,\mathrm{lb/ft^3}$, the viscosity $\nu=1.1\times10^{-5}\,\mathrm{ft^2/s}$, as well as the specific mass, which changes only in the buoyancy force. The forcing term (56) actually appears for the Weissenberg number $We=2.1484\times10^{-4}$ ($\lambda=0.5$) and due to the heating of a vertical wall of the duct, while the horizontal walls remain adiabatic (Figure 1). Then the Reynolds and Rossby numbers only change with the effect of the velocity scale, which is chosen as the fully developed mean longitudinal velocity

$$W_0=\frac{1}{A}\int_\Omega w\,\mathrm{d}\Omega$$

Copyright © 2008 John Wiley & Sons, Ltd.

DOI: 10.1002/fld

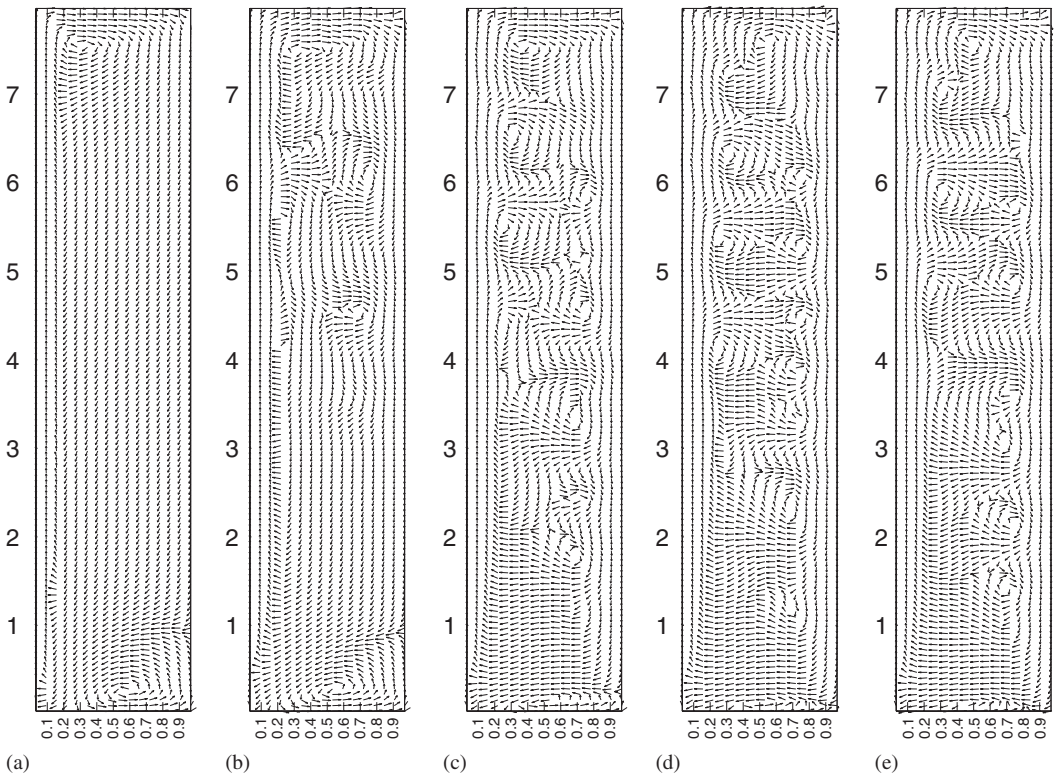

Figure 14. Secondary flow in a duct 8:1, for t: (a) 10 s; (b) 500 s; (c) 1600 s; (d) 3500 s; and (e) fully developed, for $Re=251$, $Ro=21.5$ ($\omega=0.005\,\text{rad/s}, G=2\times10^{-4}\,\text{lb/ft}^3$), $We=2.1484\times10^{-4}$, $Gr=170000$, $Pr=8$.

This scene is typical for the flow of a rotating Newtonian fluid without buoyancy forces [4] and for the flow of an isothermal rotating weakly viscoelastic fluid, presented in the Figures 5 and 6. In this situation, the only varying parameter is the Grashof number. The Prandtl number is fixed in $Pr=8$, that corresponds to a saturated water state.

The temperature at the exterior wall is initially considered null. The temperature at the interior wall of the transversal section of the duct is kept at 33°F. The initial velocity is the same given in the last section, that is, $u(0)=0, v(0)=0, w(0)=w_1$, where w_1 is solution of the equation of Poisson $-\nabla^2=-G/\rho$ with non-slip condition at the walls of the duct.

In Figure 10, is exhibited $Gr=54330$ a transient structure of the normalized velocity of secondary flows for the Grashof number. The streamlines for the same times are presented in the Figure 11.

It can be observed that, in the time until $t=100$ s (Figure 12(a)), the rotation effects predominate and the corresponding isotherms show that the temperature was not established in the domain. As time evolves, the mixed convection appears once the isotherms in (b), (c) and (d) of the Figure 12 are developing for bigger times. This type of convection influences the flow until the obtention of a structure flow where the recirculations, in the transversal section of the duct, are leaned in

Copyright © 2008 John Wiley & Sons, Ltd.

DOI: 10.1002/fld

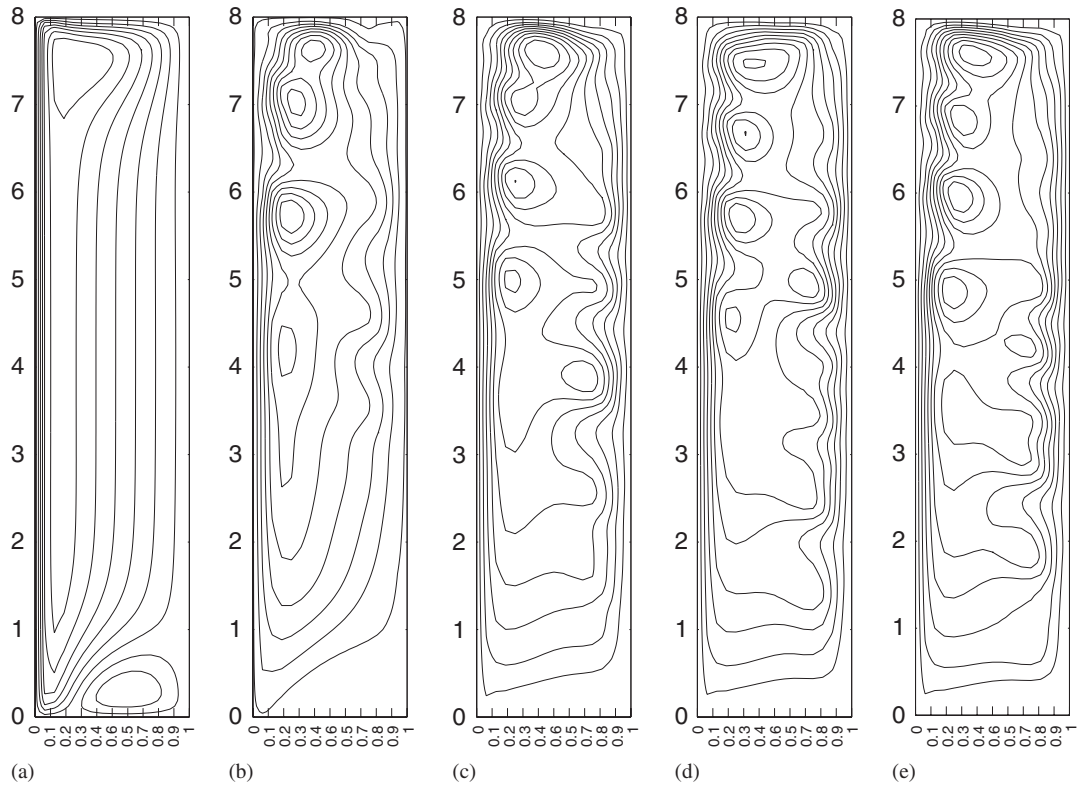

Figure 15. Streamlines of the secondary flow in a duct with aspect ratio 8:1 for t: (a) 10 s; (b) 500 s; (c) 1600 s; (d) 3500 s; and (e) fully developed, for $Re=251$, $Ro=21.5$ ($\omega=0.005\,\mathrm{rad/s}$, $G=2\times10^{-4}\,\mathrm{lb/ft^3}$), $We=2.1484\times10^{-4}$, $Gr=170000$, $Pr=8$.

the lower and upper parts of the duct, giving place to another type of recirculation that encloses almost all the transversal section. This happens in the interval of time of 1000–1600 s, as can be seen in the Figures 10(c), (d) and 11(c) and (d). A great difference exists with the structure of a fully developed isothermal flow considered in the last section and shown in Figure 5.

We also observe that the two vortex structure is broken due to the buoyancy force. In Figure 11, is shown the streamlines of this flow in the transversal section. It is possible to observe that the recirculations near the upper wall are stronger that the ones at the lower wall.

In Figure 13, the profiles of the longitudinal velocity of the fully developed flow can be observed and compared with the velocity profiles without rotation. These profiles show a different effect than would be expected. The horizontal profile, in the center of the transversal section (Figure 13), is greater than the velocity profile without mixed convection (Figure 6). However, at the lower and upper walls, it diminishes in the absence of the convective force, even though the flow rate of this fluid structure is 97% in comparison to the initial outflow.

When the Grashof number is increased to $Gr=170000$, the evolution of the secondary flow shows the onset of certain instabilities of the structure of the previous secondary flow. This can be observed in Figures 14 and 15 for the streamlines. The appearance of small recirculations can

Copyright © 2008 John Wiley & Sons, Ltd.

DOI: 10.1002/fld

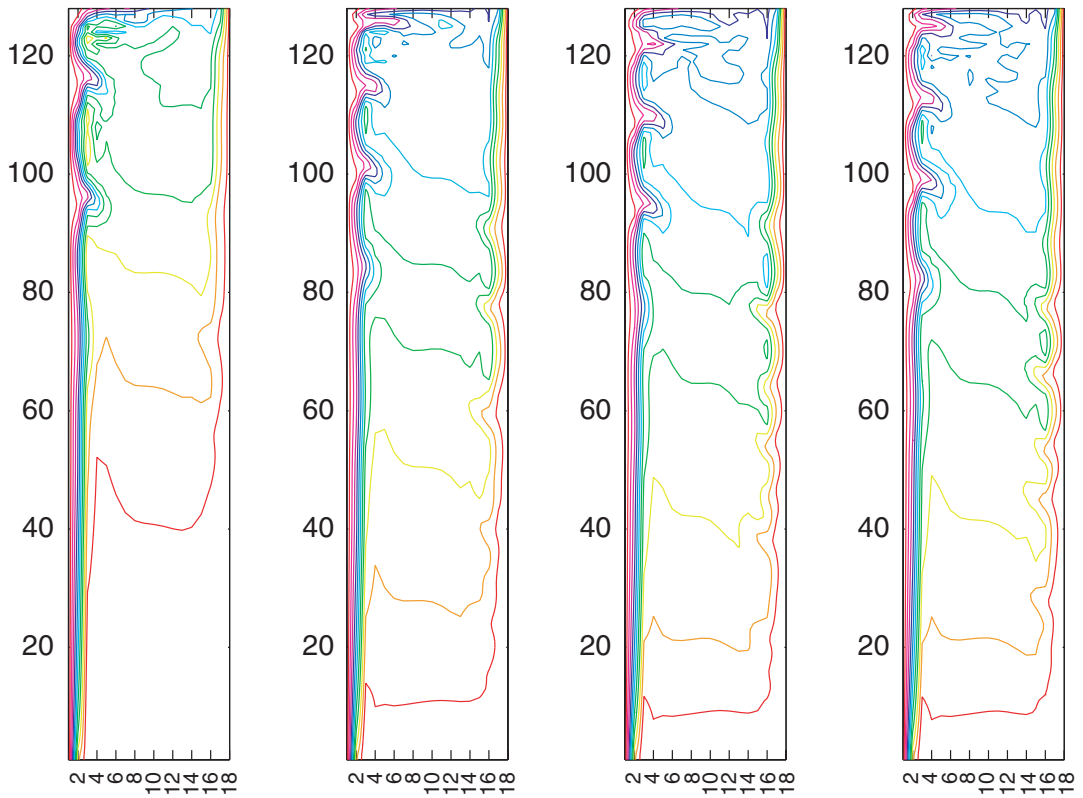

Figure 16. Isotherms in a duct 8:1 for t: (a) 500 s; (b) 1600 s; (c) 3500 s; and (d) fully developed, for $Re=251$, $Ro=21.5$, $We=2.1484\times10^{-4}$, $Gr=170000$, $Pr=8$.

be appreciated, but almost all are in the same direction. The only recirculation in the opposite direction is at the lower wall. But this one only appears at the time $t=10$ s; at other times it is very weak and even disappears at later times, as can be observed in Figure 15.

In Figure 16, the isotherms were obtained for the same times as the ones for which the velocity fields were calculated. These isotherms are very similar to the ones of natural convection with ducts of high aspect ratio [8]. We observe that, in this situation, the buoyancy force is the predominant one and neutralizes the effects of the Coriolis force (Figure 17).

8. CONCLUSIONS

A numeric study has been conducted for the internal flow of a weakly viscoelastic fluid in a rotating rectangular duct subject to a buoyancy force. The numerical method of finite differences was employed in primitive variables with a Neumann condition for the pressure on a staggered grid.

Copyright © 2008 John Wiley & Sons, Ltd.

DOI: 10.1002/fld

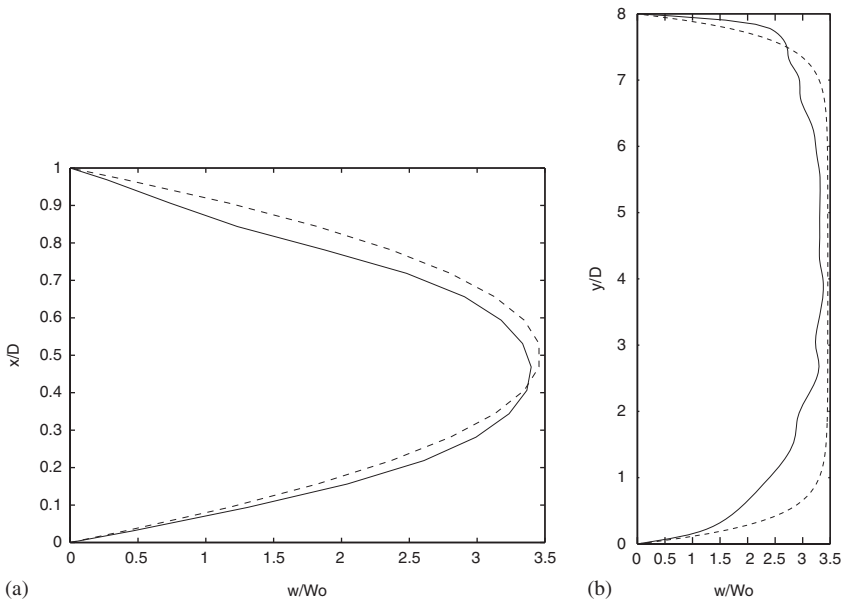

Figure 17. Axial velocity profiles in a duct 8:1: (a) horizontal ($y/D=4$) and (b) vertical ($x/D=0.5$) [dashed line ($\omega=0$), continuous line ($\omega=0.005$ rad/s)] for $Re=251$, $Ro=21.5$, $We=2.1484\times10^{-4}$, $Gr=170\,000$, $Pr=8$, $Q_t/Q=0.9391$, $u_{\max}/w_{\max}=0.0847$.

Numerical simulations for the cases of a rotating weakly viscoelastic flow with and without mixed convection have been carried out by using a direct velocity–pressure algorithm which solves the Poisson equation for the pressure without any iteration. This equation is time-dependent due to the incorporation of the velocity field through the Neumann condition for the pressure.

Without natural convection, the numerical results for ducts with aspect ratio 2:1 and 8:1 show that when the Weissenberg number increases ($We>7.4\times10^{-5}$), the configuration of the secondary flow contains multiple vortexes until a double vortex configuration is achieved, as predicted by Speziale [4].

For the first case, the numeric results for ducts with aspect ratio 2:1 and 8:1 show that when the Weissenberg number increases ($We>7.4\times10^{-5}$), the secondary flow is restabilized to a stretched double vortex configuration, which was predicted by Speziale [4].

The numerical results for the second case, with ducts of aspect ratio 8:1, show that the buoyancy forces neutralize the effects of the Coriolis force.

Special attention was given to the transient development of the structures of the fields in this study. The reason for the study is that the literature does not contain much information about these cases. The numerical scheme developed in this work for a rotating flow can be employed for larger scales in geophysical problems as well as with porous walls [12, 29–32].

ACKNOWLEDGEMENTS

We thank CNPq for support and the referees for their important comments and suggestions.

Copyright © 2008 John Wiley & Sons, Ltd.

DOI: 10.1002/fld

REFERENCES

1. Claeyssen JR, Bravo E, Platte R. Simulation in primitive variables of incompressible flow with pressure Neumann condition. *International Journal for Numerical Methods in Fluids* 1999; **30**:1009–1026.
2. Gresho PM, Sani RL. On pressure boundary conditions for the incompressible Navier–Stokes equations. *International Journal for Numerical Methods in Fluids* 1987; **7**:1111–1145.
3. Chen HB, Nandakumar K, Finlay WH, Ku HC. Three-dimensional viscous flow through rotating channel: a pseudospectral matrix method approach. *International Journal for Numerical Methods in Fluids* 1996; **23**: 379–396.
4. Speziale CG. Numerical study of viscous flow in rotating rectangular ducts. *Journal of Fluid Mechanics* 1982; **122**:251–271.
5. Speziale CG. Numerical solution of rotating internal flows. *Lecture Notes in Applied Mathematics* 1985; **22**: 261–288.
6. Robertson AM. On viscous flow in curved pipes of non-uniform cross-section. *International Journal for Numerical Methods in Fluids* 1996; **22**:771–798.
7. Khayat RE. On overstability in thermal convection of viscoelastic fluids. *Developments in Non-Newtonian Flows AMD* 1993; **175**:71–83.
8. Jin YY, Chen CF. Instability of convection and heat transfer of high Prandtl number fluids in a vertical slot. *Journal of Heat Transfer* 1996; **118**:359–365.
9. Nonino C, Comini G. An equal-order velocity–pressure algorithm for incompressible thermal flows, part 1: formulation. *Numerical Heat Transfer*, *Part B* 1997; **32**:1–15.
10. Nonino C, Croce G. An equal-order velocity–pressure algorithm for incompressible thermal flows, part 2: validation. *Numerical Heat Transfer*, *Part B* 1997; **32**:17–35.
11. Liqiu W. Buoyancy-force-driven transitions in flow structures and their effects on heat transfer in rotating curved channel. *International Journal of Heat and Mass Transfer* 1997; **40**(2):223–235.
12. Lee KT, Yan WM. Mixed convection heat and mass transfer in radially rotating rectangular ducts. *Numerical Heat Transfer*, *Part A* 1998; **34**:747–767.
13. Lee E, Lee YH, Pai YT, Hsu JP. Flow of a viscoelastic shear-thinning fluid between two concentric rotating spheres. *Chemical Engineering Science* 2002; **57**:507–514.
14. Park HM, Hong SM, Lim JY. Estimation of rheological parameters using velocity measurements. *Chemical Engineering Science* 2007; **62**:6806–6815.
15. Hart JE. Instability and secondary motion in a rotating channel flow. *Journal of Fluid Mechanics* 1971; **45**: 341–351.
16. Ladyzhenskaya O. *The Mathematical Theory of Viscous Incompressible Flow*. Gordon & Breach: New York, 1969.
17. Sheu TWH, Wang MMT, Tsai SF. Pressure boundary condition for a segregated approach to solving incompressible Navier–Stokes equations. *Numerical Heat Transfer*, *Part B* 1998; **34**:457–467.
18. Harlow FH, Welch JE. Numerical calculation of time dependent viscous incompressible flow of fluid with free surface. *Physics of Fluids* 1965; **8**:2182–2189.
19. Roache PJ. *Computational Fluid Dynamics*. Hermosa Publications: Albuquerque, NM, 1982.
20. Ames WF. *Numerical Methods for Partial Differential Equations* (3rd edn). Academic Press: New York, 1992.
21. Ferziger JH, Perić M. *Computational Methods for Fluid Dynamics* (2nd edn). Springer: Berlin, 1999.
22. Abdallah S. Numerical solutions for the pressure Poisson equation with Neumann boundary conditions using a non-staggered grid. *Journal of Computational Physics* 1987; **70**:182–192.
23. Alfrink BJ. On the Neumann problem for the pressure in a Navier–Stokes model. *Proceedings of the 2nd International Conference on Numerical Methods in Laminar and Turbulent Flow*, Venice, 1981; 389–399.
24. Morse PM, Feschbach H. *Methods of Theoretical Physics*, *Part I*. McGraw-Hill: New York, 1953.
25. Temam R. *Navier–Stokes Equations*, *Theory and Numerical Analysis* (3rd edn). North-Holland: Amsterdam, 1984 (reprint AMS Chelsea Publishing, Providence, RI, 2004).
26. Ferguson J, Kemblowski Z. *Applied Fluid Rheology*. Elsevier Applied Science: London, 1991.
27. Joseph DD. *Fluid Dynamics of Viscoelastic Liquids*. Springer: New York, 1990.
28. Claeyssen JR, Bravo E, Rubio O. Rotating incompressible flow with a pressure Neumann condition. *International Journal for Numerical Methods in Fluids* 2006; **50**:1–26.
29. Yang Z. Large eddy simulation of fully developed turbulent flow in a rotating pipe. *International Journal for Numerical Methods in Fluids* 2000; **33**:681–694.

Copyright © 2008 John Wiley & Sons, Ltd.

DOI: 10.1002/fld

30. Govatsos PA, Papantonis DE. A characteristic based method for the calculation of three-dimensional incompressible, turbulent and steady flows in hydraulic turbomachines and installations. *International Journal for Numerical Methods in Fluids* 2000; **34**:1–30.
31. Vanyo PJ. *Rotating Fluids in Engineering and Science*. Dover Publications, Inc.: Mineola, New York, 1993.
32. Yamaguchi H, Fujiyoshi J, Matsui H. Spherical Couette flow of a viscoelastic fluid. Part I: experimental study of the inner sphere rotation. *Journal of Non-Newtonian Fluid Mechanics* 1997; **69**:29–46.

Copyright © 2008 John Wiley & Sons, Ltd.

DOI: 10.1002/fld